

Spatiotemporal Continual Learning for Mobile Edge UAV Networks: Mitigating Catastrophic Forgetting

Chuan-Chi Lai, *Member, IEEE*

Abstract—This paper addresses the critical challenge of coordinating mobile edge UAV networks to maintain robust service in highly dynamic spatiotemporal environments. Conventional Deep Reinforcement Learning (DRL) approaches often suffer from catastrophic forgetting when transitioning between distinct task scenarios, such as moving from dense urban clusters to sparse rural areas. These transitions typically necessitate computationally expensive retraining or model resets to adapt to new user distributions, leading to service interruptions. To overcome these limitations, we propose a computationally efficient Spatiotemporal Continual Learning (STCL) framework realized through a Group-Decoupled Multi-Agent Proximal Policy Optimization (G-MAPPO) algorithm. Our approach integrates a novel Group-Decoupled Policy Optimization (GDPO) mechanism that utilizes dynamic z -score normalization to autonomously balance heterogeneous objectives, including energy efficiency, user fairness, and coverage. This mechanism effectively mitigates gradient conflicts induced by concept drifts without requiring offline retraining. Furthermore, the framework leverages the 3D mobility of UAVs as a spatial compensation layer, enabling the swarm to autonomously adjust altitudes to accommodate extreme density fluctuations. Extensive simulations demonstrate that the proposed STCL framework achieves superior resilience, characterized by an elastic recovery of service reliability to approximately 0.95 during phase transitions. Compared to the MADDPG baseline, G-MAPPO not only prevents knowledge forgetting but also delivers an effective capacity gain of 20% under extreme traffic loads, validating its potential as a scalable solution for edge-enabled aerial swarms.

Index Terms—Mobile Edge Computing (MEC), Spatiotemporal Continual Learning, Catastrophic Forgetting, UAV Swarms, Computational Efficiency, Group-Decoupled Policy Optimization (GDPO).

I. INTRODUCTION

IN recent years, the deployment of Unmanned Aerial Vehicles as Aerial Base Stations (UAV-BSs) has emerged as a transformative solution for enhancing the coverage and capacity of next-generation wireless networks [1]. Compared to conventional terrestrial infrastructure, UAV-BSs offer superior mobility and the ability to establish Line-of-Sight (LoS) communication links through flexible 3D positioning [2]. These distinct advantages render them pivotal for addressing

This research was supported by the National Science and Technology Council, Taiwan, under Grant No. NSTC 114-2221-E-194-062-. This work was also partially supported by the Advanced Institute of Manufacturing with High-tech Innovations (AIM-HI) from the Featured Areas Research Center Program within the framework of the Higher Education Sprout Project by the Ministry of Education (MOE) in Taiwan. (*Corresponding author: Chuan-Chi Lai*)

C.-C. Lai is with the Department of Communications Engineering, National Chung Cheng University, Minxiong Township, Chiayi County 621301, Taiwan, and also with the Advanced Institute of Manufacturing with High-tech Innovations (AIM-HI), National Chung Cheng University, Minxiong Township, Chiayi County 621301, Taiwan (e-mail: chuanclai@ccu.edu.tw).

temporary traffic surges [3], restoring emergency communications in disaster-stricken zones, and bridging coverage gaps in remote regions [4], [5], [6].

Despite their potential, the practical orchestration of UAV swarms faces significant challenges stemming from the highly dynamic and non-stationary nature of user distributions. Real-world mobile traffic exhibits strong spatiotemporal tidal effects, where user density shifts drastically over time, such as the migration from dense urban business districts to sparse suburban residential areas [7]. When traditional Multi-Agent Reinforcement Learning (MARL) algorithms are employed to navigate these transitions, they frequently suffer from *catastrophic forgetting*. This phenomenon occurs when agents overwrite previously learned optimal policies while adapting to new environments, leading to severe performance degradation and service instability during task transitions [8].

For instance, consider a UAV swarm transitioning between a dense urban stadium and a sparse rural highway. In the urban scenario, the optimal policy requires agents to practice interference mitigation by carefully adjusting transmission power and 3D positioning to serve crowded users without causing co-channel interference. Conversely, in the rural scenario, the objective shifts to coverage maximization, compelling agents to adopt aggressive transmission strategies to reach distant users. Catastrophic forgetting manifests when the swarm, after adapting to the rural environment, loses its previously learned delicate interference management skills. Consequently, if the swarm encounters a sudden traffic surge or returns to an urban-like cluster, it naively applies the aggressive rural policy, leading to severe interference storms and network paralysis.

Compounding this challenge is the rigorous requirement to simultaneously balance multiple heterogeneous objectives, specifically energy efficiency, user fairness, and minimum Quality of Service (QoS) guarantees. These objectives often possess conflicting gradients and varying physical magnitudes, which can destabilize the learning process through destructive interference [9]. To address such environmental shifts, existing adaptive strategies typically rely on periodic offline retraining or transfer learning with extensive fine-tuning [10]. However, such approaches incur prohibitive computational overhead and latency, rendering them ill-suited for real-time online coordination where rapid responsiveness is paramount.

To bridge this gap, this paper proposes a resilient Spatiotemporal Continual Learning (STCL) framework realized through a Group-Decoupled Multi-Agent Proximal Policy Optimization (G-MAPPO) algorithm. Unlike conventional methods that depend on external intervention, our framework features native resilience that enables the swarm to autonomously adapt to spatiotemporal variations. The primary contributions of this

work are as follows:

- We introduce the Group-Decoupled Policy Optimization (GDPO) mechanism. Beyond simple normalization, this mechanism utilizes gradient projection to orthogonalize and balance conflicting objectives. This ensures stable policy updates even when the magnitude of reward signals fluctuates significantly across distinct environments.
- We exploit the 3D vertical mobility of UAVs as a physical spatial compensation layer. By allowing UAVs to autonomously adjust their altitudes within a range of 80 m to 120 m, the swarm can dynamically expand or contract its service footprint to effectively counter extreme variations in user density [2], [11].
- We conduct extensive stress tests with up to 140 users across a sequential task chain consisting of urban, suburban, and rural scenarios. The simulation results demonstrate that the proposed framework achieves an elastic recovery of service reliability and provides an effective capacity gain of approximately 20% compared to the state-of-the-art MADDPG baseline, effectively mitigating catastrophic forgetting without requiring task-specific resets.

The remaining sections of this paper are organized as follows. Section II reviews related work on UAV deployment, MARL for UAV swarms, and continual learning in wireless networks. Section III presents the system model and problem formulation. Section IV details the proposed STCL framework and the GDPO mechanism. Section V discusses the simulation setup and performance evaluation. Finally, Section VI concludes the paper and outlines future research directions.

II. RELATED WORK

A. UAV Deployment and 3D Trajectory Design

UAV deployment optimization has been investigated extensively to maximize coverage probability and spectral efficiency. Early channel modeling studies established the fundamental analytical relationship between UAV altitude and air-to-ground path loss probabilities [2]. Subsequent research focused on optimizing 3D placement to decouple coverage and capacity constraints in heterogeneous networks [12]. Additionally, studies investigated coverage overlapping to optimize service for arbitrary user crowds in 3D space [13]. To address operational limitations, energy-efficient trajectory designs were proposed to balance propulsion consumption with throughput requirements [14]. Moreover, adaptive deployment approaches were developed to enhance fairness and balance offload traffic across multi-UAV networks [15].

Recent studies extended these concepts to 3D scenarios by formulating mixed-integer nonconvex problems to minimize energy consumption while optimizing the number of deployed UAVs [16]. Furthermore, interference-aware path planning strategies were developed to enhance aerial user connectivity by mitigating line-of-sight interference [17]. To address conflicting objectives involving energy consumption, risk, and path length in dynamic urban environments, advanced evolutionary algorithms were proposed for adaptive multi-objective path planning [18]. Beyond algorithmic optimization,

architectural advancements integrated trajectory adaptation as xApps within the Open-Radio Access Network (O-RAN) framework, explicitly targeting information freshness and network sustainability [19].

However, most conventional approaches rely on convex optimization or heuristic algorithms requiring perfect Channel State Information (CSI) and assuming static user distributions. Although recent frameworks integrated 3D mobility, altitude is frequently treated as a fixed parameter or an independent optimization variable [11]. Consequently, these models often lack the coupling required for autonomous adaptation in environments with rapid spatiotemporal variations in user density [7].

B. Multi-Agent Reinforcement Learning for UAV Swarms

Multi-Agent Reinforcement Learning (MARL) is widely adopted to manage dynamic environment complexity. The Multi-Agent Deep Deterministic Policy Gradient (MADDPG) algorithm [20] is extensively applied to enable decentralized UAVs to learn cooperative policies for interference management and trajectory control [21], [22]. More recently, Multi-Agent Proximal Policy Optimization (MAPPO) [23] demonstrated superior performance in cooperative tasks due to its on-policy update mechanism. To address scalability during dynamic cluster reconfiguration, Hierarchical Multi-Agent DRL (H-MADRL) frameworks were introduced to jointly optimize power allocation and mobility management [24].

Furthermore, spatiotemporal-aware DRL architectures incorporating Transformer mechanisms were developed to capture complex environmental dynamics and guarantee deterministic communication requirements during cooperative coverage tasks [25]. Resource allocation frameworks based on these algorithms showed significant throughput gains over static baselines [26]. Despite these advancements, standard MARL formulations face challenges when simultaneously optimizing heterogeneous metrics such as fairness, delay, and energy. Conflicting gradients among these objectives often cause training instability [9]. Although hybrid approaches combining Lyapunov optimization with DRL address queue stability under heterogeneous traffic demands [27], these methods typically rely on model-based constraints. Moreover, these algorithms are typically validated in stationary environments. When user distributions shift distinctively, such as during transitions from urban to rural scenarios, standard baselines frequently suffer policy degradation and fail to maintain service reliability.

C. Continual Learning and Adaptation in Wireless Networks

Continual Learning (CL) methodologies are pivotal for addressing the stability-plasticity dilemma in dynamic systems, ensuring agents acquire new capabilities without catastrophic forgetting of consolidated knowledge. In non-stationary wireless networks, adapting to time-varying traffic patterns is critical for maintaining persistent Quality of Service. Deep transfer learning architectures have enhanced cellular traffic prediction by transferring feature representations from data-rich sources to data-sparse target regions [28]. Similarly, within UAV

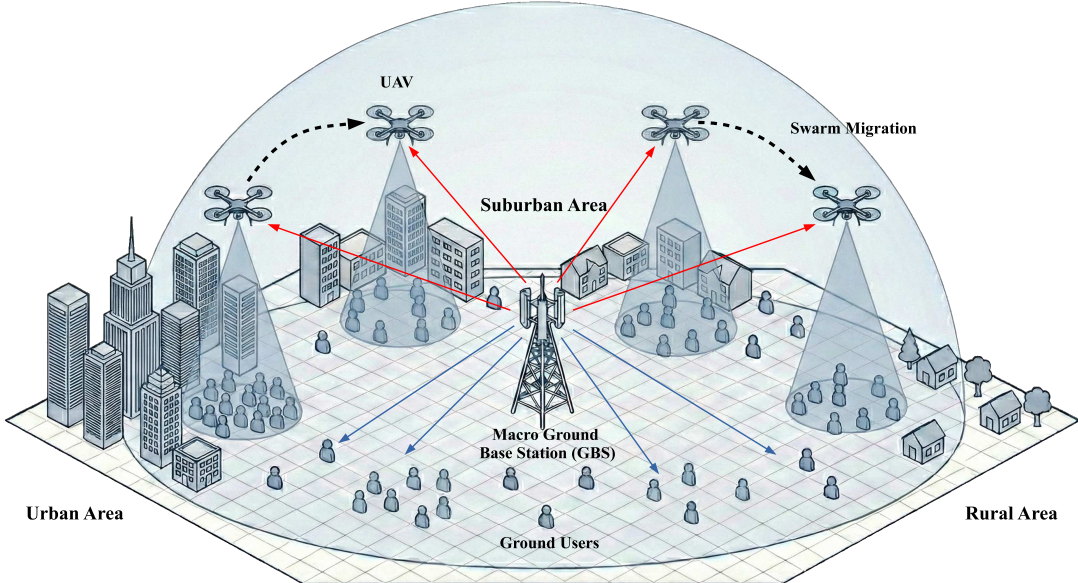


Fig. 1. Illustration of the 3D aerial-ground integrated network deployed across a heterogeneous environment. The service area features a spatial transition from a dense Urban Area (left), through a Suburban Area (center), to a sparse Rural Area (right). A central Macro Ground Base Station (GBS) provides ubiquitous omnidirectional coverage (hemispherical dome), while multiple UAVs function as mobile small cells. The dashed arrows illustrate the spatiotemporal migration of the UAV swarm, emphasizing its continuous adaptation to shifting user densities.

networks, continuous transfer learning mechanisms facilitate trajectory adaptation, allowing control policies to be progressively refined across shifting environmental conditions [10]. Additionally, regularization-based techniques constrain parameter updates to preserve essential feature information.

Nevertheless, existing solutions predominantly rely on periodic offline retraining, parameter isolation, or experience replay buffers necessitating substantial memory resources [29]. Such methods frequently incur prohibitive computational latency and assume distinct task boundaries, rendering them impractical for real-time online deployment where rapid responsiveness is paramount. In contrast, this study proposes a framework for native resilience. By integrating Group-Decoupled Policy Optimization (GDPO) [30] with physical 3D spatial compensation, the system achieves online autonomous adaptation to spatiotemporal concept drifts. This approach eliminates the need for explicit task detection or computationally intensive retraining.

III. SYSTEM MODEL AND PROBLEM FORMULATION

A. 3D Aerial-Ground Network Architecture

Consider a downlink aerial-ground integrated network comprising N rotary-wing Unmanned Aerial Vehicles (UAVs) functioning as aerial base stations, and M ground users distributed over a geographical area of interest $\mathcal{D} \subset \mathbb{R}^2$. The set of UAVs is denoted by $\mathcal{U} = \{1, \dots, N\}$, and the set of ground users is denoted by $\mathcal{M} = \{1, \dots, M\}$. The overall system scenario is illustrated in Fig. 1.

Unlike conventional 2D deployment models, the UAVs in this framework possess 3D mobility to facilitate spatial adaptation. The instantaneous position of the i -th UAV at time step t is represented by a 3D coordinate vector

$\mathbf{q}_i(t) = [x_i(t), y_i(t), h_i(t)]^T$, where $[x_i(t), y_i(t)]$ denotes the horizontal position and $h_i(t)$ represents the altitude. To ensure operational safety and regulatory compliance, the altitude is constrained within a predefined range $H_{\min} \leq h_i(t) \leq H_{\max}$. This vertical degree of freedom allows the network to dynamically expand or contract the service footprint in response to varying user densities.

To provide ubiquitous coverage and backhaul support, a macro Ground Base Station (GBS) is deployed at the center of the service area, located at $\mathbf{q}_{\text{GBS}} = [x_{\text{GBS}}, y_{\text{GBS}}, H_{\text{GBS}}]^T$. The GBS operates with a transmit power P_{GBS} , which is significantly higher than the UAV transmit power P_{UAV} . The GBS serves as an anchor node for users outside the effective coverage of the UAVs. Consequently, the network forms a heterogeneous two-tier architecture in which the UAV swarm acts as a mobile small-cell tier that complements the static macro-cell tier. Furthermore, we assume the wireless backhaul links between the UAVs and the GBS utilize a dedicated high-frequency band with sufficient capacity. Therefore, the backhaul transmission is considered ideal and does not constitute a bottleneck for the downlink access performance.

B. Terrestrial Channel Model for GBS

For the communication link between the macro GBS and ground user u , we adopt a standard terrestrial path loss model that accounts for urban shadowing effects. The path loss $L_{\text{GBS},u}(t)$ in dB is modeled as:

$$L_{\text{GBS},u}(t) = \text{PL}(d_0) + 10\kappa \log_{10} \left(\frac{d_{\text{GBS},u}(t)}{d_0} \right) + \chi_{\sigma}, \quad (1)$$

where $d_{\text{GBS},u}(t)$ is the Euclidean distance between the GBS and user u , d_0 is the reference distance, and κ is the path loss

exponent. Typically, $\kappa \approx 3.5 \sim 4$ for urban non-LoS (NLoS) environments. The term $\chi_\sigma \sim \mathcal{N}(0, \sigma^2)$ represents log-normal shadowing with a standard deviation of σ .

Unlike the UAV links that may benefit from high LoS probabilities, the GBS link is dominantly NLoS due to low antenna height and dense building blockage. This distinct propagation characteristic motivates the deployment of UAVs to provide coverage extension and capacity offloading for edge users.

C. Probabilistic Air-to-Ground Channel Model

The communication links between UAVs and ground users are modeled using a probabilistic Line-of-Sight (LoS) channel model, which accounts for the blockage effects caused by urban obstacles. The probability of establishing an LoS link between the i -th UAV and the u -th user depends on the elevation angle $\theta_{i,u}(t) = \arctan\left(\frac{h_i(t)}{r_{i,u}(t)}\right)$, where $r_{i,u}(t)$ is the horizontal distance. The LoS probability is given by [2]:

$$P_{\text{LoS}}(\theta_{i,u}(t)) = \frac{1}{1 + a \cdot \exp(-b(\theta_{i,u}(t) - a))}, \quad (2)$$

where a and b are environment-dependent constants. The corresponding NLoS probability is defined as $P_{\text{NLoS}} = 1 - P_{\text{LoS}}$. The average path loss is then formulated as:

$$\bar{L}_{i,u}(t) = P_{\text{LoS}} \cdot L_{i,u}^{\text{LoS}}(t) + P_{\text{NLoS}} \cdot L_{i,u}^{\text{NLoS}}(t), \quad (3)$$

where $L_{i,u}^{\text{LoS}}$ and $L_{i,u}^{\text{NLoS}}$ incorporate the free-space path loss along with additional attenuation factors η_{LoS} and η_{NLoS} , respectively.

D. User Association and SINR

Each ground user u associates with the node providing the strongest reference signal power, which can be either a UAV or the GBS. Let $k \in \mathcal{U} \cup \{\text{GBS}\}$ denote the serving node. The received Signal-to-Interference-plus-Noise Ratio (SINR) for user u at time t is expressed as:

$$\gamma_u(t) = \frac{P_k G_{k,u}(t)}{\sigma^2 + \sum_{j \neq k} P_j G_{j,u}(t)}, \quad (4)$$

where P_k is the transmit power and σ^2 is the noise power. The term $G_{k,u}(t)$ represents the effective channel gain, defined as:

$$G_{k,u}(t) = G_k^{\text{ant}} \cdot 10^{-\bar{L}_{k,u}(t)/10}, \quad (5)$$

where $\bar{L}_{k,u}(t)$ is the path loss derived in the previous subsections. Specifically, we assume the GBS employs a static omnidirectional antenna with a constant gain $G_{\text{GBS}}^{\text{ant}}$, while UAVs are equipped with downlink antennas having gain $G_{\text{UAV}}^{\text{ant}}$. This user association strategy dynamically offloads traffic from the GBS to the UAV swarm based on proximity and instantaneous channel conditions.

E. Spatiotemporal User Distribution Models

To emulate the non-stationary nature of real-world traffic, the spatial distribution of ground users, which is denoted by the probability density function (PDF) $\Phi(\mathbf{w})$, varies according to a sequential task chain. Three distinct spatial models are defined to represent the Urban, Suburban, and Rural environments.

1) *Crowded Urban Scenario (T_{Urban})*: The urban environment is characterized by high user density concentrated in specific hotspots, such as business districts or stadiums. This distribution is modeled using a Thomas Cluster Process (TCP), which is a specialized form of the Poisson Cluster Process. In this model, parent points representing cluster centers are generated with intensity λ_p , and daughter points representing users are distributed around each parent according to an isotropic Gaussian distribution with variance σ_u^2 . The PDF for a user location \mathbf{w} is given by:

$$\Phi_U(\mathbf{w}) = \frac{1}{K} \sum_{k=1}^K \frac{1}{2\pi\sigma_u^2} \exp\left(-\frac{|\mathbf{w} - \mathbf{c}_k|^2}{2\sigma_u^2}\right), \quad (6)$$

where K is the number of hotspots, \mathbf{c}_k denotes the center of the k -th cluster, and σ_u controls the spread of the cluster to represent the hotspot radius.

2) *Suburban Scenario (T_{Suburban})*: The suburban environment represents a transition state with moderate user density. This phase features a combination of residential clusters and scattered users. This distribution is modeled using a Gaussian Mixture Model (GMM) combined with a uniform background component, defined as follows:

$$\Phi_S(\mathbf{w}) = \alpha \cdot \frac{1}{|\mathcal{D}|} + (1 - \alpha) \sum_{k=1}^{K'} \pi_k \mathcal{N}(\mathbf{w} | \boldsymbol{\mu}_k, \boldsymbol{\Sigma}_k), \quad (7)$$

where $\alpha \in [0, 1]$ represents the proportion of background users, $|\mathcal{D}|$ is the area of the region, π_k is the weight of the k -th cluster, and $\mathcal{N}(\cdot)$ denotes the Gaussian density function. This composite model effectively captures the spatial heterogeneity typically found in semi-urbanized regions.

3) *Rural Scenario (T_{Rural})*: The rural environment is characterized by sparse user density and a notable lack of distinct hotspots. The user locations are modeled using a Homogeneous Poisson Point Process (HPPP), which results in a uniform distribution over the service area \mathcal{D} . The PDF is defined as:

$$\Phi_R(\mathbf{w}) = \begin{cases} \frac{1}{|\mathcal{D}|}, & \text{if } \mathbf{w} \in \mathcal{D}, \\ 0, & \text{otherwise.} \end{cases} \quad (8)$$

This scenario serves to evaluate the coverage maximization capability of the UAV swarm when users are widely dispersed across the geographical area.

F. Problem Formulation

The primary objective of this study is to learn a joint control policy π that maximizes the long-term system utility across sequential spatiotemporal tasks. The global utility $U_{\text{total}}(t)$ is formulated as a composite metric that reflects multiple performance indicators, including throughput, fairness, and coverage. The optimization problem is mathematically formulated as follows:

$$\max_{\pi} \mathbb{E} \left[\sum_{t=0}^T \gamma^t U_{\text{total}}(t) \right] \quad (9)$$

subject to the following physical and operational constraints:

$$C1: H_{\min} \leq h_i(t) \leq H_{\max}, \quad \forall i \in \mathcal{U}, \forall t, \quad (10)$$

$$C2: \mathbf{q}_i^{xy}(t) \in \mathcal{D}, \quad \forall i \in \mathcal{U}, \forall t, \quad (11)$$

$$C3: |\mathbf{q}_i(t) - \mathbf{q}_j(t)| \geq d_{\min}, \quad \forall i \neq j, \forall t, \quad (12)$$

where $\gamma \in [0, 1)$ denotes the discount factor.

The constraints are defined as follows:

- **C1** enforces the flight altitude constraints to comply with regulatory limits and specific communication requirements.
- **C2** restricts the horizontal movement of the UAVs to remain within the designated service region \mathcal{D} .
- **C3** imposes a collision avoidance constraint, which ensures that the Euclidean distance between any pair of UAVs remains above a minimum safety threshold d_{\min} to prevent physical accidents.

The utility function U_{total} incorporates conflicting objectives such as Energy Efficiency (EE), User Fairness (Jain's Index), and Coverage Rate. The presence of these diverse metrics necessitates a sophisticated optimization strategy that is capable of balancing these trade-offs while strictly adhering to the safety constraints defined above.

IV. PROPOSED SPATIOTEMPORAL CONTINUAL LEARNING (STCL) FRAMEWORK

A. Framework Overview

To achieve robust orchestration of UAV swarms in highly dynamic and non-stationary environments, we propose the Spatiotemporal Continual Learning (STCL) Framework based on G-MAPPO, as illustrated in Fig. 2. This framework adopts the Centralized Training with Decentralized Execution (CTDE) paradigm, which effectively reconciles the need for global coordination during learning with the constraints of local scalability during deployment.

The architecture comprises two primary neural components:

- **Decentralized Actor (π_θ):** Operating locally on each UAV, the Actor maps partial observations $o_i(t)$, such as relative coordinates and local topology, to a probability distribution over the discrete 3D action space. This design ensures that real-time decision-making is computationally lightweight and independent of global communication, satisfying the low-latency requirements of edge deployment.
- **Centralized Critic (V_ϕ):** Active solely during the training phase, the Critic leverages global state information $s(t)$, which encapsulates the joint configuration of the swarm and user distributions. By evaluating the global value function, the Critic guides the Actors' gradient updates, effectively mitigating the non-stationarity and partial observability issues inherent in multi-agent learning.

A distinguishing feature of this framework is the integration of the Group-Decoupled Policy Optimization (GDPO) module. Unlike standard MAPPO, which sums raw rewards directly, GDPO introduces a dynamic scalarization layer. This mechanism addresses the *reward scale imbalance* caused by environmental phase transitions (e.g., from capacity-centric

Urban to coverage-centric Rural), ensuring consistent policy improvement without manual weight tuning.

B. POMDP Formulation for Edge UAV Networks

The decision-making process is modeled as a Decentralized Partially Observable Markov Decision Process (Dec-POMDP), defined by the tuple $\langle \mathcal{U}, \mathcal{S}, \mathcal{A}, \mathcal{O}, \mathcal{P}, \mathcal{R}, \gamma \rangle$, where \mathcal{U} is the set of UAV agents; \mathcal{S} is global state space, representing the joint configuration of UAVs and users; \mathcal{A} is joint action space, comprising discrete 3D movement commands for each UAV; \mathcal{O} is joint observation space, capturing local sensory inputs for each UAV; \mathcal{P} is state transition probability function; \mathcal{R} is reward function, designed to reflect multiple performance objectives; and γ is the discount factor.

1) *Observation Space (\mathcal{O}):* Constrained by onboard sensing limits, each UAV i receives a local observation $o_i(t)$ representing a partial view of the global state $s(t)$. The observation vector is defined as:

$$o_i(t) = \{\mathbf{q}_i(t), \mathbf{v}_i(t), \mathcal{I}_{\text{neigh}}^i(t), \mathcal{M}_{\text{cov}}^i(t)\}, \quad (13)$$

where $\mathbf{q}_i(t)$ and $\mathbf{v}_i(t)$ denote the UAV's 3D kinematics; $\mathcal{I}_{\text{neigh}}^i(t)$ encodes the relative positions of neighbors for collision avoidance; and $\mathcal{M}_{\text{cov}}^i(t)$ represents the local channel state information (CSI) of served ground users.

To ensure rapid convergence in the complex 3D control manifold, we discretize the action space. At each timestep t , each UAV i selects a discrete action $a_i(t) \in \mathcal{A}$:

$$\mathcal{A} = \{\Delta x_{\pm}, \Delta y_{\pm}, \Delta h_{\pm}, \text{Hover}\}. \quad (14)$$

In this formulation, Δx_{\pm} and Δy_{\pm} govern horizontal traversal, whereas Δh_{\pm} facilitates vertical spatial adaptation. The term 'Hover' denotes the stationary action where the UAV maintains its current 3D coordinates (i.e., a zero-displacement vector). This capability allows agents to preserve energy when positioned at an optimal coverage point, while the vertical mobility remains critical for maximizing Line-of-Sight (LoS) probability in rural scenarios and mitigating co-channel interference within dense urban clusters.

C. Heterogeneous Reward Composition

To fulfill the multi-objective requirements of the spatiotemporal system, we design a composite reward structure. The raw reward vector for agent i consists of five distinct physical components:

$$\mathbf{r}_i^{\text{raw}}(t) = [r_{\text{EE}}, r_{\text{Fair}}, r_{\text{Load}}, r_{\text{Cov}}, r_{\text{QoS}}]^T. \quad (15)$$

Let $\mathcal{K} = \{\text{EE, Fair, Load, Cov, QoS}\}$ denote the set of heterogeneous objectives to be optimized. The specific components are defined as follows:

- r_{EE} (Energy Efficiency): Ratio of system throughput to total power consumption.
- r_{Fair} (Jain's Fairness Index): Promotes equitable data rates among users.
- r_{Load} (Load Balance): Penalizes variance in user association numbers across UAVs.

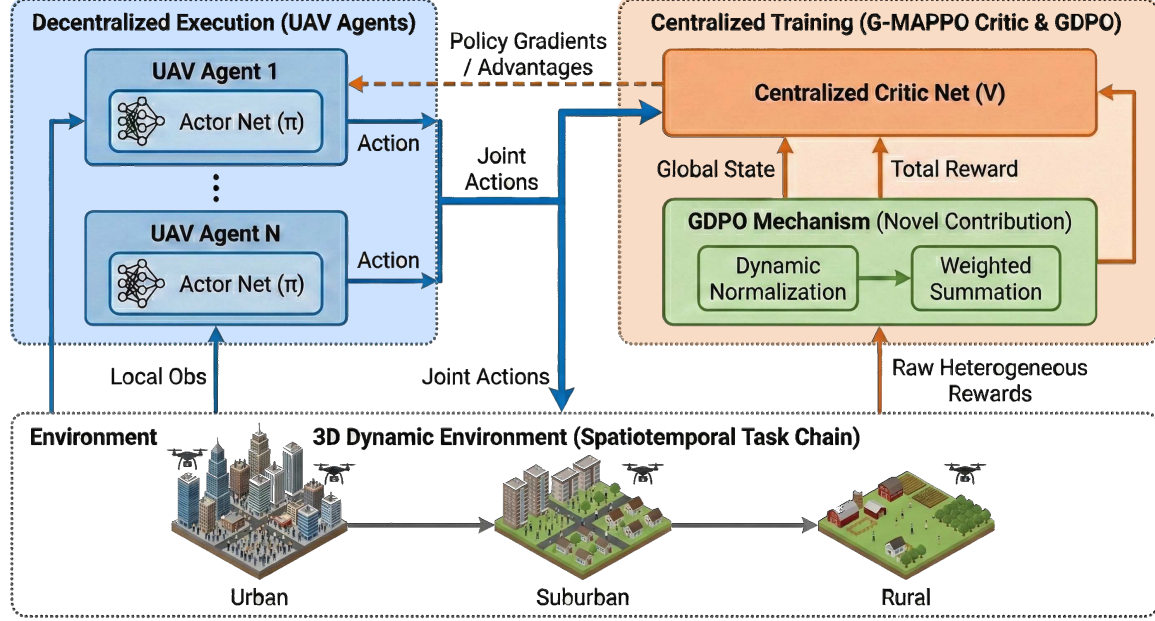


Fig. 2. Schematic overview of the proposed Spatiotemporal Continual Learning (STCL) framework. The architecture leverages a Group-Decoupled Multi-Agent Proximal Policy Optimization (G-MAPPO) approach within a Centralized Training with Decentralized Execution (CTDE) paradigm. A key innovation is the Group-Decoupled Policy Optimization (GDPO) mechanism (highlighted in green), which dynamically normalizes heterogeneous reward signals from the non-stationary 3D environment. This ensures stable scalar feedback for the centralized critic, mitigating catastrophic forgetting across varying spatiotemporal tasks.

- r_{Cov} (Coverage Rate): Percentage of users satisfying the minimum SINR threshold.
- r_{QoS} (QoS Penalty): A penalty applied when the worst-case user rate falls below a critical threshold.

Additionally, a collision penalty r_{col} is imposed if safety distances are violated.

D. Group-Decoupled Policy Optimization (GDPO)

A critical challenge in this continual learning setting is the gradient dominance phenomenon arising from the scale disparity of heterogeneous rewards. For instance, r_{EE} (Mbps/W) may vary by orders of magnitude compared to $r_{\text{Fair}} \in [0, 1]$. Direct summation leads to optimization instability, where large-scale objectives overshadow small-scale ones, causing catastrophic forgetting when tasks switch.

The GDPO mechanism resolves this by dynamically normalizing rewards based on their running statistics. Let $\mu_k(t)$ and $\sigma_k(t)$ be the running mean and standard deviation of the k -th reward component. The normalized reward $\hat{r}_k(t)$ is computed as:

$$\hat{r}_k(t) = \frac{r_k^{\text{raw}}(t) - \mu_k(t)}{\sigma_k(t) + \epsilon}, \quad (16)$$

where ϵ is a stability constant. The final scalar reward $R_{\text{total}}(t)$ is then derived via a weighted summation:

$$R_{\text{total}}(t) = \sum_{k \in \mathcal{K}} w_k \cdot \hat{r}_k(t) - \eta \cdot \mathbb{I}_{\text{col}}, \quad (17)$$

where w_k are preference weights and \mathbb{I}_{col} is the collision indicator. By decoupling the magnitude from the semantic importance, GDPO ensures that the policy remains sensitive to all objectives regardless of the current environmental phase.

E. G-MAPPO Learning Algorithm

The complete training procedure is outlined in Algorithm 1. The process iterates through three phases:

1) *Phase 1: Decentralized Data Collection:* In each iteration, the UAV swarm interacts with the environment to collect trajectories. Crucially, the system records the raw reward vectors $\mathbf{r}_i^{\text{raw}}(t)$ rather than a pre-summed scalar. This preserves the distributional information of each objective necessary for the subsequent GDPO step.

2) *Phase 2: GDPO-Based Reward Scalarization:* Before the Generalized Advantage Estimation (GAE) step, the raw rewards undergo GDPO processing (Lines 6-8). The algorithm updates the running statistics (μ_k, σ_k) for each component and computes the normalized scalar reward $R_{\text{total}}(t)$ according to (17). This dynamic normalization effectively "bleaches" the environmental scale shifts, providing a stationary learning signal to the Critic.

3) *Phase 3: Centralized Optimization:* With the scalarized rewards $R_{\text{total}}(t)$ derived from the GDPO mechanism, the generalized advantage estimation (GAE) is employed to compute the advantage function \hat{A}_t and the target value V_t^{target} . The centralized critic then minimizes the value loss $\mathcal{L}(\phi) = \mathbb{E}[(V_{\phi}(s_t) - V_t^{\text{target}})^2]$. Simultaneously, the actor network is updated by maximizing the PPO-clipped objective function:

$$\begin{aligned} \mathcal{L}(\theta) = \mathbb{E} \left[\min \left(\rho_t(\theta) \hat{A}_t, \right. \right. \\ \left. \left. \text{clip}(\rho_t(\theta), 1 - \epsilon, 1 + \epsilon) \hat{A}_t \right) \right] + \sigma \mathcal{H}(\pi_{\theta}), \end{aligned} \quad (18)$$

Algorithm 1: G-MAPPO: Spatiotemporal Continual Learning with GDPO

Input: Task sequence \mathcal{T} , Max episodes M , Horizon T_{hor}

Output: Optimized policy π_θ and value function V_ϕ

Init: Initialize π_θ, V_ϕ ; Initialize GDPO scalers $\Sigma_k = \{\mu_k, \sigma_k\}$

1 **for** episode $e = 1$ to M **do**

 // Task Adaptation

 2 Set user distribution Φ for current task $T \in \mathcal{T}$

 3 Reset environment, observe initial \mathbf{o}

 4 $\mathcal{B} \leftarrow \emptyset$

 // Phase 1: Trajectory Collection

 5 **for** $t = 1$ to T_{hor} **do**

 6 **for** agent $i \in \mathcal{U}$ **do**

 7 | Sample action $a_i(t) \sim \pi_\theta(\cdot | o_i(t))$

 8 | Execute $\mathbf{a}(t)$, observe s' and raw rewards $\mathbf{r}^{\text{raw}}(t)$

 9 | Execute $\mathbf{a}(t)$, observe s' and raw rewards $\mathbf{r}^{\text{raw}}(t)$

 10 | // Phase 2: GDPO Normalization

 11 | **for** objective $k \in \mathcal{K}$ **do**

 12 | | Update statistics $\{\mu_k, \sigma_k\}$ using $r_k^{\text{raw}}(t)$

 13 | | $\hat{r}_k(t) \leftarrow (r_k^{\text{raw}}(t) - \mu_k) / (\sigma_k + \epsilon)$

 14 | $R_{\text{total}}(t) \leftarrow \sum_k w_k \hat{r}_k(t) - \eta \mathbb{I}_{\text{col}}$

 15 | Store $(s, \mathbf{o}, \mathbf{a}, R_{\text{total}}, s')$ in \mathcal{B}

 16 **end**

 // Phase 3: Optimization

 17 Compute \hat{A} via GAE using R_{total}

 18 **for** epoch = 1 to K_{opt} **do**

 19 | Sample mini-batches from \mathcal{B}

 20 | $\theta \leftarrow \theta + \alpha \nabla_\theta \mathcal{L}_{\text{PPO}}(\theta)$

 21 | $\phi \leftarrow \phi - \beta \nabla_\phi \mathcal{L}_{\text{Value}}(\phi)$

 22 **end**

 23 Clear buffer \mathcal{B}

24 **end**

where $\rho_t(\theta) = \frac{\pi_\theta(a_t | o_t)}{\pi_{\theta_{\text{old}}}(a_t | o_t)}$ denotes the probability ratio between the current and old policies. The first term in the expectation is the surrogate objective that ensures monotonic policy improvement via the clipping parameter ϵ , while $\mathcal{H}(\pi_\theta)$ represents the entropy bonus weighted by σ to encourage spatiotemporal exploration. This formulation, combined with the stabilized reward signals from GDPO, guarantees superior sample efficiency and robust policy convergence in non-stationary environments.

V. SIMULATION RESULTS AND ANALYSIS

In this section, we evaluate the performance of the proposed G-MAPPO framework. Departing from the static simulation setups common in prior works, our evaluation specifically focuses on the algorithm's computational efficiency and its resilience to catastrophic forgetting within highly dynamic spatiotemporal environments.

TABLE I
SIMULATION PARAMETERS AND G-MAPPO HYPERPARAMETERS

Parameter	Value
<i>Spatiotemporal Environment Settings</i>	
Service Area	$2 \times 2 \text{ km}^2$
Number of UAVs (N)	4
Urban Phase User Density (M)	140 (High Load)
Rural Phase User Density (M)	40 (Low Load)
User Distribution Modeling	Gaussian Mixture Models (GMM)
UAV Altitude Range (H)	[80, 120] m
<i>Heterogeneous Communication Model</i>	
Carrier Frequency (f_c)	2 GHz
System Bandwidth (B)	20 MHz
Noise Power Density (N_0)	-174 dBm/Hz
UAV Transmit Power (P_{UAV})	23 dBm
GBS Transmit Power (P_{GBS})	43 dBm (Macro BS)
GBS Antenna Gain ($G_{\text{GBS}}^{\text{ant}}$)	15 dBi
UAV Antenna Gain ($G_{\text{UAV}}^{\text{ant}}$)	2 dBi
Path Loss Model	Probabilistic LoS/NLoS [2]
<i>G-MAPPO Learning Hyperparameters</i>	
Actor Learning Rate (α_π)	5×10^{-4}
Critic Learning Rate (α_v)	1×10^{-3}
Discount Factor (γ)	0.99
GAE Parameter (λ)	0.95
Clipping Ratio (ϵ)	0.2
Mini-batch Size	64
Optimizer	Adam
Reward Scaling Mechanism	Dynamic z -score (GDPO)

A. Simulation Setup and Performance Evaluation Metrics

The simulation parameters are summarized in Table I. We consider a mobile edge network area of $2 \times 2 \text{ km}^2$. To rigorously assess the resilience against non-stationary concept drifts, the simulation environment is designed to undergo periodic phase transitions among three distinct spatiotemporal regimes:

- 1) **Crowded Urban Phase:** Characterized by a high user density of $M = 140$ with highly clustered distributions. The primary challenges involve managing co-channel interference and capacity offloading for the GBS.
- 2) **Suburban Phase:** Features moderate user density ($M = 80 \sim 100$) with semi-clustered distributions. It requires the swarm to balance spectral efficiency with regional coverage.
- 3) **Rural Phase:** Marked by a low user density of $M = 40$ with sparse distributions. The objective shifts toward maximizing coverage probability and extending the service footprint.

The swarm size is restricted to $N = 4$ for the $2 \times 2 \text{ km}^2$ area. This sparse deployment forces agents to dynamically prioritize mission objectives, serving as a rigorous benchmark for the resilience of G-MAPPO against catastrophic forgetting compared to traditional MARL baselines.

1) *Total System Throughput:* To evaluate the aggregate network capacity across different density regimes, we measure the *Total System Throughput*, defined as the sum of achievable data rates of all served users:

$$C_{\text{total}} = \sum_{u=1}^M R_u. \quad (19)$$

This metric reflects the macroscopic service capability of the UAV swarm, serving as a primary performance indicator in interference-limited regimes where bandwidth resources are highly contested.

2) *User Fairness and Service Consistency*: To ensure equitable service distribution and prevent the network from exclusively serving users with strong channel conditions, we employ Jain's Fairness Index (JFI) on user data rates:

$$\mathcal{J}_{\text{rate}} = \frac{(\sum_{u=1}^M R_u)^2}{M \cdot \sum_{u=1}^M R_u^2}. \quad (20)$$

A higher $\mathcal{J}_{\text{rate}} \in [0, 1]$ indicates a fairer resource allocation. This metric is particularly critical for detecting service shrinkage, where an algorithm might maximize aggregate throughput by abandoning difficult-to-serve edge users.

3) *Spatial Service Reliability and Minimum QoS*: In sparse environments, the priority shifts from capacity to coverage. We utilize two complementary metrics to assess service quality:

- **Spatial Service Reliability (P_{cov})**: Defined as the ratio of users whose achievable data rate exceeds the minimum QoS threshold $R_{\text{th}} = 1$ Mbps:

$$P_{\text{cov}} = \frac{1}{M} \sum_{u=1}^M \mathbb{I}(R_u \geq R_{\text{th}}). \quad (21)$$

- **Guaranteed Minimum QoS**: We track the minimum user rate $\min(R_u)$ within the network to evaluate the worst-case service experience, ensuring that the system maintains basic connectivity even for the most remote users.

4) *UAV Fleet Load Efficiency*: To assess the coordination level of the swarm, we evaluate the load balancing efficiency among the $N+1$ nodes (including the GBS) using a JFI-based load index:

$$\mathcal{J}_{\text{load}} = \frac{(\sum_{k=0}^N M_k)^2}{(N+1) \cdot \sum_{k=0}^N M_k^2}, \quad (22)$$

where M_k is the number of users served by node k . This metric quantifies the cooperative behavior of the agents and their ability to dynamically redistribute user loads to prevent individual node bottlenecks.

5) *Total System Reward and Learning Stability*: To quantify the learning dynamics and resilience against catastrophic forgetting, we track the *Total System Reward* (Weighted Sum). Furthermore, learning stability is evaluated by the variance of the reward curve, reflecting the algorithm's robustness to non-stationary gradient noise during environmental phase transitions.

B. Learning Dynamics and Training Stability

Fig. 3 illustrates the convergence trajectory of the total system reward across the sequential task chain. This metric serves as a holistic indicator of the agents' ability to balance heterogeneous objectives under varying user densities.

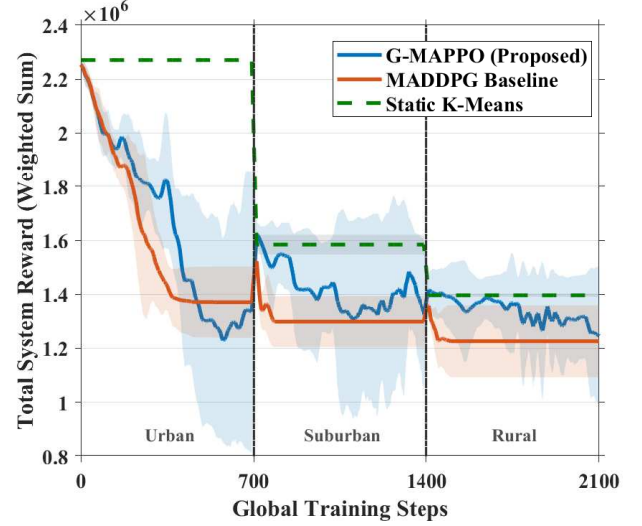


Fig. 3. Convergence analysis of the Total System Reward (Weighted Sum) across the spatiotemporal task chain (Urban → Suburban → Rural). The Static K-Means (green dashed line) serves as an idealized upper bound utilizing perfect global information. The proposed G-MAPPO (blue line) demonstrates superior learning stability and resilience, maintaining a higher reward plateau compared to the MADDPG baseline (orange line), which suffers from significant policy degradation and high variance (wide shaded regions) after the first environmental transition at Step 700.

1) *Convergence Efficiency and Environmental Impact*: It is observed that the total reward naturally exhibits a stepwise descending trend across the three phases. This corresponds to the reduction in user density from the *Urban phase* ($M = 140$) to the *Rural phase* ($M = 40$), which inherently limits the maximum achievable aggregate throughput. Within the initial *Urban phase*, the proposed G-MAPPO framework (blue line) demonstrates rapid convergence, stabilizing its policy within approximately 400 episodes. While the Static K-Means baseline (green dashed line) maintains the highest reward, it serves as an idealized upper bound by leveraging perfect global coordinate information, which is unavailable in real-time decentralized operations.

2) *Impact of GDPO on Stability*: A critical advantage of G-MAPPO is the stability of its learning curve. As shown in the *Urban* and *Suburban* phases of Fig. 3, the MADDPG baseline (orange line) exhibits a wide shaded error band, indicating high variance and unstable gradient updates. In contrast, G-MAPPO maintains a narrower variance profile. This validates the efficacy of the GDPO mechanism, which normalizes the reward scales to prevent high-magnitude objectives from destabilizing the actor-critic networks.

3) *Resilience to Task Transitions*: The resilience of the proposed framework is most evident during the transition to the *Suburban phase* (Step 700).

- **Policy Degradation in MADDPG**: The MADDPG baseline suffers from a sharp performance drop, failing to recover a competitive reward level throughout the Suburban phase. This indicates a susceptibility to catastrophic forgetting, where the model struggles to adapt to the new semi-clustered distribution.
- **Adaptive Recovery of G-MAPPO**: Conversely, G-

MAPPO exhibits a robust recovery capability. Despite the environmental shift, it maintains a reward plateau significantly higher than MADDPG, effectively bridging the gap between the theoretical upper bound (Static K-Means) and the failing baseline. This confirms that the G-MAPPO agents successfully retain generalized feature representations, allowing for consistent performance even as the environment becomes increasingly sparse.

C. Resilience Against Catastrophic Forgetting

To evaluate the agents' capability to retain learned policies under concept drift, Fig. 4 presents the Spatial Service Reliability ratio. This metric reflects the swarm's effectiveness in maintaining user connectivity above the required QoS threshold ($R_{th} = 1$ Mbps).

1) Performance under Physical Constraints (Urban Phase):

In the initial *Urban phase*, the network operates under extreme saturation ($M = 140$ users vs. $N = 4$ UAVs).

- **Baseline Stagnation:** The MADDPG baseline (orange solid line) experiences a rapid decay, flatlining at a ratio of ≈ 0.42 after Step 300. The lack of variance (narrow shaded area) suggests *policy stagnation*, where the agents settle into a suboptimal local minimum and cease attempting to serve difficult users.

- **Active Exploration:** In contrast, G-MAPPO (blue solid line) maintains a higher reliability for the first 400 steps.

Although it eventually dips due to the sheer physical impossibility of covering 140 users with limited resources, the continued variance indicates that the agents retain plasticity and are actively exploring the state space for better configurations, rather than suffering from mode collapse.

- **Elastic Recovery and Adaptation (Suburban Phase):** The most critical evidence of resilience appears at the transition to the *Suburban phase* (Step 700).

• **Superior Rebound:** Immediately following the environmental shift, G-MAPPO exhibits a powerful "elastic rebound," with reliability surging to ≈ 0.95 , closely matching the **Static K-Means upper bound (green dashed line)**. This indicates that the agents successfully utilized generalized feature representations to instantly adapt to the new distribution.

• **Comparison:** While MADDPG also recovers, its peak only reaches ≈ 0.85 , and it quickly settles into a static lower bound (≈ 0.7). This confirms that G-MAPPO possesses superior *adaptation agility*, allowing it to recover optimal service levels faster and more effectively than the baseline.

3) *Stability vs. Agility (Rural Phase):* In the final *Rural phase* (Step 1400), the Static K-Means baseline drops to ≈ 0.65 , reflecting the geometric difficulty of covering widely dispersed users. MADDPG maintains a flat trajectory (≈ 0.6), again indicative of a static policy serving a fixed subset of users. G-MAPPO exhibits higher fluctuations; however, these variations reflect the active 3D load-balancing maneuvers (further analyzed in Section V-D2), where agents dynamically

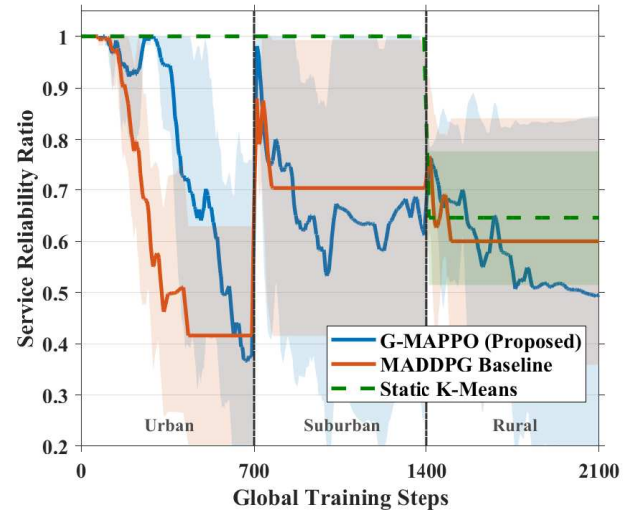


Fig. 4. Evolution of the Spatial Service Reliability (P_{cov}) across spatiotemporal phases. The Static K-Means (green dashed line) represents the theoretical upper bound. In the dense Urban phase, both RL algorithms degrade due to physical capacity constraints ($M = 140$); however, G-MAPPO (blue solid line) exhibits active exploration compared to the rapid policy stagnation of the MADDPG baseline (orange solid line). Notably, at the transition to the Suburban phase (Step 700), G-MAPPO demonstrates a superior "elastic rebound," recovering to near-optimal reliability, thereby verifying its resilience against catastrophic forgetting.

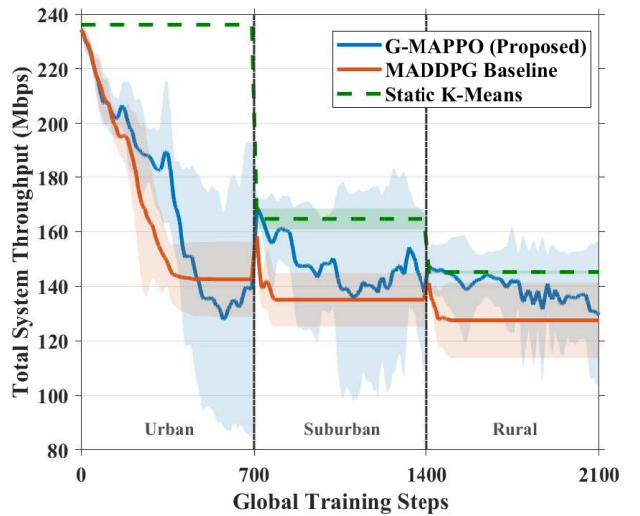


Fig. 5. Evolution of the Total System Throughput across spatiotemporal phases. The throughput naturally correlates with user density, decreasing from the Urban ($M = 140$) to the Rural ($M = 40$) phase. In the Rural phase, the MADDPG baseline (orange line) appears to achieve higher throughput; however, this is a misleading artifact of selective service, where the baseline maximizes rate by serving only proximal users. In contrast, G-MAPPO (blue line) prioritizes broader coverage (as shown in Fig. 4), accepting a trade-off in aggregate throughput to maintain connectivity for distant edge users.

adjust altitudes to maximize fleet-wide efficiency rather than settling for static, localized coverage.

D. Multi-Objective Performance Trade-offs

Beyond basic connectivity, the quality of service is evaluated through system throughput, fairness, and the guaranteed

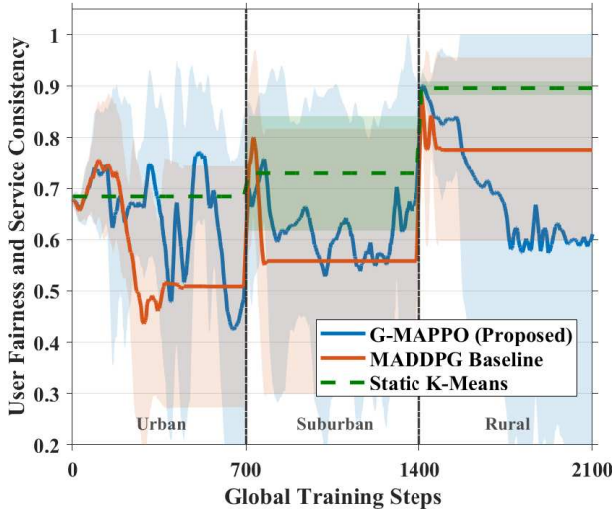


Fig. 6. Evolution of the Service Distribution Consistency (Jain's Fairness Index). In the interference-limited Urban phase, G-MAPPO (blue line) maintains a fairness index competitive with the Static K-Means upper bound, demonstrating effective interference mitigation. In the Rural phase, the high fairness index observed for MADDPG (orange line) is a result of survivorship bias, as the index is calculated only among the subset of served users. G-MAPPO exhibits realistic fairness fluctuations, reflecting its active dynamic readjustment to balance service between central and edge users.

minimum user rate. Fig. 5, Fig. 6, and Fig. 7 present the performance evolution of these metrics.

1) *Throughput, Fairness, and User-Centric QoS*: The analysis of *Total System Throughput* (Fig. 5) and *Service Distribution Consistency* (Fig. 6) reveals distinct strategic behaviors.

- **Urban Phase:** In the interference-limited Urban regime ($M = 140$), G-MAPPO maintains a competitive system throughput level comparable to the Static K-Means upper bound. Notably, the JFI index for G-MAPPO fluctuates but generally stays above the MADDPG baseline, indicating that the GDPO mechanism successfully prevents the policy from over-fitting to strong users at the expense of weaker ones.

- **The Rural Paradox:** In the Rural phase, MADDPG appears to achieve higher throughput and fairness. However, this is a misleading indicator of superiority. As evidenced by the low coverage ratio in Fig. 4, MADDPG's high per-user rate is achieved by *service shrinkage*, which entails serving only a small cluster of proximate users while dropping distant connections. G-MAPPO, by maintaining a larger service footprint, naturally incurs a penalty in aggregate throughput due to path loss from serving edge users, reflecting a strategic choice to prioritize mission completion over raw rate maximization.

2) *UAV Fleet Load Efficiency*: To interpret the underlying coordination logic, we analyze the *UAV Fleet Load Efficiency* in Fig. 8. This metric quantifies how effectively the user load is distributed among the swarm nodes.

- **Coordination Decay in Baseline**: The MADDPG baseline (orange line) suffers from severe coordination decay, particularly in the Suburban and Rural phases. The declining efficiency suggests that the agents, having lost

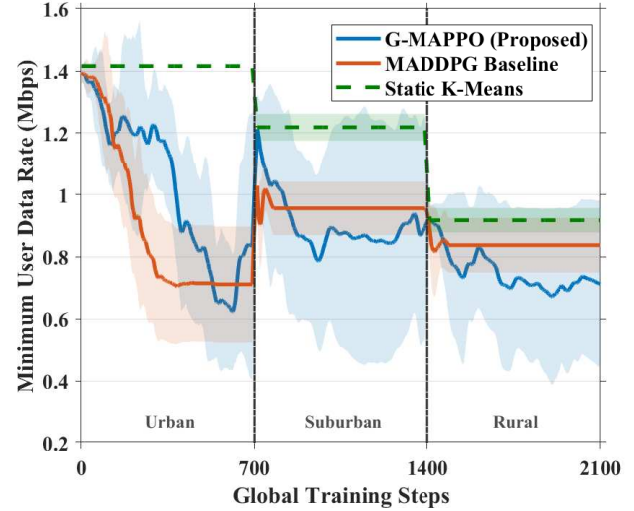


Fig. 7. Evolution of the Guaranteed Minimum QoS (Minimum User Data Rate) across spatiotemporal phases. In the Urban phase, G-MAPPO (blue line) effectively mitigates interference, maintaining a higher minimum rate for the worst-case users compared to the MADDPG baseline (orange line). In the Rural phase, MADDPG exhibits a deceptively higher minimum rate; this is an artifact of service shrinkage, where the baseline abandons distant users to maintain high rates for a smaller active subset, whereas G-MAPPO incurs a penalty for maintaining connectivity to edge users.

their generalized policy, fail to form a cohesive network, leading to a scenario where resources are critically misallocated.

- **Active Balancing in G-MAPPO**: Conversely, G-MAPPO (blue line) maintains a robust load efficiency index (> 0.75) throughout the task chain. This provides the physical explanation for the variance observed in Fig. 4: the fluctuations in coverage are not signs of instability, but rather evidence of active load-balancing maneuvers. By dynamically adjusting altitudes and positions to redistribute users, G-MAPPO ensures that no single UAV becomes a bottleneck, a capability essential for the long-term sustainability of battery-constrained edge networks.

3) *Summary of Strategic Trade-offs*: In conclusion, the simulation results highlight a fundamental trade-off. While the MADDPG baseline succumbs to catastrophic forgetting, which manifests as policy stagnation, service shrinkage, and poor load distribution, the proposed G-MAPPO framework leverages GDPO to maintain robust adaptability. Although G-MAPPO may exhibit lower peak throughput in sparse regimes compared to the selectively optimizing baseline, it delivers superior coverage reliability, load balancing, and training stability, thereby establishing itself as the more viable solution for practical, mission-critical UAV edge networks.

E. Scalability and Stress Resilience Analysis

To rigorously assess the operational limits of the proposed framework, Fig. 9 presents a stress test of the Spatial Service Reliability ratio across varying user densities ranging from $M = 60$ (light load) to $M = 140$ (extreme saturation).

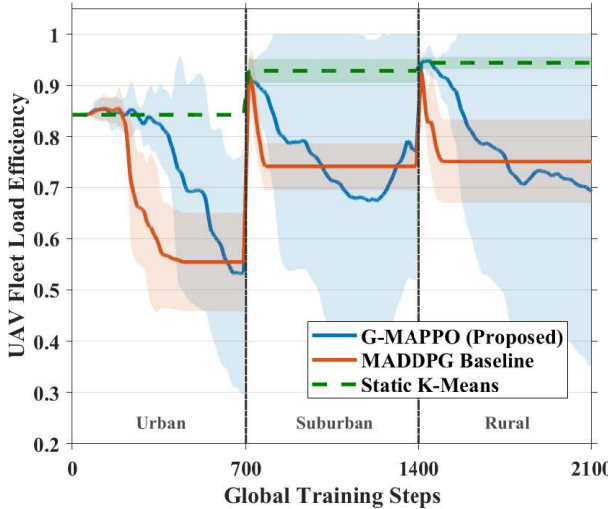


Fig. 8. Evolution of the UAV Fleet Load Efficiency index across spatiotemporal phases. The MADDPG baseline (orange line) exhibits a continuous decline in load balancing efficiency, dropping below 0.6 in the Rural phase. This indicates a breakdown in cooperative behavior, where some UAVs become overloaded while others remain idle. In contrast, G-MAPPO (blue line) maintains a high efficiency index (> 0.75), confirming that the agents actively coordinate 3D positions to redistribute user load, thereby preventing individual node bottlenecks and extending fleet endurance.

1) *Graceful Degradation under Load*: As the user density increases, the system exhibits a pattern of graceful degradation rather than catastrophic failure.

- **Light to Moderate Load**: At $M = 60$ (cyan line) and $M = 80$ (blue line), G-MAPPO maintains near-optimal reliability (> 0.9) across most phases, effectively fully covering the service area.
- **Extreme Saturation**: At $M = 140$ (red line), the network is physically saturated (35 users per UAV). Despite this, G-MAPPO prevents total system collapse, stabilizing at a reliability ratio of ≈ 0.5 in the Rural phase. This indicates that even under extreme stress, the agents intelligently prioritize a sustainable subset of connections rather than randomly dropping service.

2) *Effective Capacity Expansion*: A critical cross-comparison highlights the superior resource efficiency of the proposed method.

- **Surpassing the Baseline at Higher Loads**: The G-MAPPO performance at $M = 120$ (orange solid line) consistently meets or exceeds the reliability of the MADDPG baseline at $M = 100$ (gray dashed line), particularly during the Suburban and Rural phases.
- **Quantifiable Gain**: This implies that G-MAPPO provides an **effective capacity gain of approximately 20%**, allowing the same physical infrastructure (4 UAVs) to serve significantly more users while maintaining a quality of service comparable to the baseline. This scalability is a direct result of the GDPO mechanism, which ensures that gradient updates remain effective even when the reward landscape becomes sparse and noisy due to high user congestion.

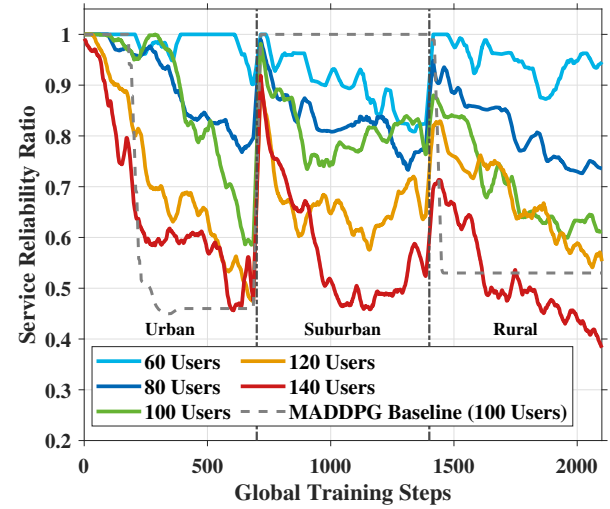


Fig. 9. Scalability analysis of the Spatial Service Reliability ratio under varying user densities ($M \in [60, 140]$). The system exhibits graceful degradation as the load increases. Notably, the proposed G-MAPPO with 120 users (orange line) consistently outperforms the MADDPG baseline with only 100 users (gray dashed line), particularly in the Suburban and Rural phases. This demonstrates that G-MAPPO effectively expands the network's operational capacity through superior interference management and policy generalization.

VI. CONCLUSION

This paper addresses catastrophic forgetting in multi-UAV edge networks operating within highly dynamic environments. We propose a Spatiotemporal Continual Learning (STCL) framework based on the G-MAPPO algorithm. By integrating Group-Decoupled Policy Optimization (GDPO), the framework orthogonalizes conflicting gradients to effectively mitigate interference among heterogeneous objectives, including coverage maximization, interference management, and energy efficiency.

Comprehensive simulations across a sequential Urban \rightarrow Suburban \rightarrow Rural task chain validate the framework's superiority. First, it demonstrates significantly lower reward variance than the MADDPG baseline, proving that gradient projection effectively regularizes policy updates. Second, the agents exhibit rapid elastic recovery at phase transitions, restoring service reliability to near-optimal levels (≈ 0.95) immediately after the Suburban shift, whereas the baseline suffers stagnation. Third, the framework achieves superior fleet-wide coordination through active 3D positioning, preventing the service shrinkage phenomenon observed in baselines that abandon edge users to maximize local throughput.

These results confirm the STCL framework as a scalable, robust solution for mission-critical aerial networks, delivering an effective capacity gain of approximately 20% under high user loads. Future work will extend this framework to decentralized onboard training with limited computational resources and explore integrating Reconfigurable Intelligent Surfaces (RIS) to enhance coverage under varying channel conditions [31], [32].

REFERENCES

[1] M. Mozaffari, W. Saad, M. Bennis, Y.-H. Nam, and M. Debbah, "A tutorial on uavs for wireless networks: Applications, challenges, and open problems," *IEEE Communications Surveys & Tutorials*, vol. 21, no. 3, pp. 2334–2360, 2019.

[2] A. Al-Hourani, S. Kandeepan, and S. Lardner, "Optimal lap altitude for maximum coverage," *IEEE Wireless Communications Letters*, vol. 3, no. 6, pp. 569–572, 2014.

[3] C.-C. Lai, C.-T. Chen, and L.-C. Wang, "On-demand density-aware uav base station 3d placement for arbitrarily distributed users with guaranteed data rates," *IEEE Wireless Communications Letters*, vol. 8, no. 3, pp. 913–916, 2019.

[4] J. Liang, J. Zhao, C. Wang, X. Yang, K. Yue, and W. Li, "Enhancing the robustness of uav search path planning based on deep reinforcement learning for complex disaster scenarios," *IEEE Transactions on Vehicular Technology*, vol. 75, no. 1, pp. 392–404, 2026.

[5] X. Zheng, G. Sun, J. Li, J. Wang, Q. Wu, D. Niyato, and A. Jamalipour, "Uav swarm-enabled collaborative post-disaster communications in low altitude economy via a two-stage optimization approach," *IEEE Transactions on Mobile Computing*, vol. 24, no. 11, pp. 11 833–11 851, 2025.

[6] T. Do-Duy, L. D. Nguyen, T. Q. Duong, S. R. Khosravirad, and H. Claussen, "Joint optimisation of real-time deployment and resource allocation for uav-aided disaster emergency communications," *IEEE Journal on Selected Areas in Communications*, vol. 39, no. 11, pp. 3411–3424, 2021.

[7] S. Troia, G. Sheng, R. Alvizu, G. A. Maier, and A. Pattavina, "Identification of tidal-traffic patterns in metro-area mobile networks via matrix factorization based model," in *2017 IEEE International Conference on Pervasive Computing and Communications Workshops (PerCom Workshops)*, 2017, pp. 297–301.

[8] J. Kirkpatrick, R. Pascanu, N. Rabinowitz, J. Veness, G. Desjardins, A. A. Rusu, K. Milan, J. Quan, T. Ramalho, A. Grabska-Barwinska, D. Hassabis, C. Clopath, D. Kumaran, and R. Hadsell, "Overcoming catastrophic forgetting in neural networks," *Proceedings of the National Academy of Sciences*, vol. 114, no. 13, pp. 3521–3526, 2017.

[9] C. Liu, X. Xu, and D. Hu, "Multiobjective reinforcement learning: A comprehensive overview," *IEEE Transactions on Systems, Man, and Cybernetics: Systems*, vol. 45, no. 3, pp. 385–398, 2015.

[10] C. Sun, G. Fontanesi, S. B. Chetty, X. Liang, B. Canberk, and H. Ahmadi, "Continuous transfer learning for uav communication-aware trajectory design," in *2024 11th International Conference on Wireless Networks and Mobile Communications (WINCOM)*, 2024, pp. 1–7.

[11] M. Alzenad, A. El-Keyi, F. Lagum, and H. Yanikomeroglu, "3-d placement of an unmanned aerial vehicle base station (uav-bs) for energy-efficient maximal coverage," *IEEE Wireless Communications Letters*, vol. 6, no. 4, pp. 434–437, 2017.

[12] M. Mozaffari, W. Saad, M. Bennis, and M. Debbah, "Efficient deployment of multiple unmanned aerial vehicles for optimal wireless coverage," *IEEE Communications Letters*, vol. 20, no. 8, pp. 1647–1650, 2016.

[13] C.-C. Lai, L.-C. Wang, and Z. Han, "The coverage overlapping problem of serving arbitrary crowds in 3d drone cellular networks," *IEEE Transactions on Mobile Computing*, vol. 21, no. 3, 2022.

[14] Y. Zeng and R. Zhang, "Energy-efficient uav communication with trajectory optimization," *IEEE Transactions on Wireless Communications*, vol. 16, no. 6, pp. 3747–3760, 2017.

[15] C.-C. Lai, Bhola, A.-H. Tsai, and L.-C. Wang, "Adaptive and fair deployment approach to balance offload traffic in multi-uav cellular networks," *IEEE Transactions on Vehicular Technology*, vol. 72, no. 3, pp. 3724–3738, 2023.

[16] H. Gong, B. Huang, and B. Jia, "Energy-efficient 3-d uav ground node accessing using the minimum number of uavs," *IEEE Transactions on Mobile Computing*, vol. 23, no. 12, pp. 12 046–12 060, 2024.

[17] U. Challita, W. Saad, and C. Bettstetter, "Interference management for cellular-connected uavs: A deep reinforcement learning approach," *IEEE Transactions on Wireless Communications*, vol. 18, no. 4, pp. 2125–2140, 2019.

[18] R. Xu, Z. Huang, C. Wang, and H. Yan, "Evolving collaborative differential evolution for dynamic multi-objective uav path planning," *IEEE Transactions on Vehicular Technology*, pp. 1–13, 2025.

[19] I. Aryendu, S. Arya, and Y. Wang, "Aura-green: Aerial utility-driven route adaptation for green cooperative networks," *IEEE Transactions on Vehicular Technology*, pp. 1–18, 2025.

[20] R. Lowe, Y. Wu, A. Tamar, J. Harb, P. Abbeel, and I. Mordatch, "Multi-agent actor-critic for mixed cooperative-competitive environments," in *Proceedings of the 31st International Conference on Neural Information Processing Systems*, Long Beach, California, USA, 2017, pp. 6382–6393.

[21] J. Liu, X. Zhao, P. Qin, F. Du, Z. Chen, H. Zhou, and J. Li, "Joint uav 3d trajectory design and resource scheduling for space-air-ground integrated power iot: A deep reinforcement learning approach," *IEEE Transactions on Network Science and Engineering*, vol. 11, no. 3, pp. 2632–2646, 2024.

[22] S. Wu, W. Xu, F. Wang, G. Li, and M. Pan, "Distributed federated deep reinforcement learning based trajectory optimization for air-ground cooperative emergency networks," *IEEE Transactions on Vehicular Technology*, vol. 71, no. 8, pp. 9107–9112, 2022.

[23] C. Yu, A. Velu, E. Vinitsky, J. Gao, Y. Wang, A. Bayen, and Y. Wu, "The surprising effectiveness of ppo in cooperative multi-agent games," in *Proceedings of the 36th International Conference on Neural Information Processing Systems*, New Orleans, LA, USA, 2022.

[24] I. A. Meer, K.-L. Besser, M. Ozger, D. A. Schupke, H. V. Poor, and C. Cavdar, "Hierarchical multi-agent drl-based dynamic cluster reconfiguration for uav mobility management," *IEEE Transactions on Cognitive Communications and Networking*, vol. 12, pp. 4957–4971, 2026.

[25] G. Chen, G. Zhao, C. Xu, Z. Han, and S. Yu, "Spatiotemporal-aware deep reinforcement learning for multi-uav cooperative coverage in emergency deterministic communications," *IEEE Transactions on Vehicular Technology*, vol. 75, no. 1, pp. 1310–1321, 2026.

[26] J. Cui, Y. Liu, and A. Nallanathan, "Multi-agent reinforcement learning-based resource allocation for uav networks," *IEEE Transactions on Wireless Communications*, vol. 19, no. 2, pp. 729–743, 2020.

[27] L. T. Hoang, C. T. Nguyen, H. D. Le, and A. T. Pham, "Adaptive 3d placement of multiple uav-mounted base stations in 6g airborne small cells with deep reinforcement learning," *IEEE Transactions on Networking*, vol. 33, no. 4, pp. 1989–2004, 2025.

[28] C. Zhang, H. Zhang, J. Qiao, D. Yuan, and M. Zhang, "Deep transfer learning for intelligent cellular traffic prediction based on cross-domain big data," *IEEE Journal on Selected Areas in Communications*, vol. 37, no. 6, pp. 1389–1401, 2019.

[29] C. H. Liu, Z. Chen, J. Tang, J. Xu, and C. Piao, "Energy-efficient uav control for effective and fair communication coverage: A deep reinforcement learning approach," *IEEE Journal on Selected Areas in Communications*, vol. 36, no. 9, pp. 2059–2070, 2018.

[30] S.-Y. Liu, X. Dong, X. Lu, S. Diao, P. Belcak, M. Liu, M.-H. Chen, H. Yin, Y.-C. F. Wang, K.-T. Cheng, Y. Choi, J. Kautz, and P. Molchanov, "Gdpo: Group reward-decoupled normalization policy optimization for multi-reward rl optimization," 2026. [Online]. Available: <https://arxiv.org/abs/2601.05242>

[31] H. Peng, Y.-T. Lin, C.-Y. Ho, and L.-C. Wang, "Energy efficiency optimization for iot systems with reconfigurable intelligent surfaces: A self-supervised reinforcement learning approach," *IEEE Transactions on Wireless Communications*, vol. 24, no. 9, pp. 7761–7776, 2025.

[32] A. M. Huroon, Y.-C. Huang, and L.-C. Wang, "Uav-ris assisted multiuser communications through transmission strategy optimization: Gbd application," *IEEE Transactions on Vehicular Technology*, vol. 73, no. 6, pp. 8584–8597, 2024.



Chuan-Chi Lai (Member, IEEE) received the Ph.D. degree in Computer Science and Information Engineering from the National Taipei University of Technology, Taiwan, in 2017. He held research and faculty positions at National Chiao Tung University and Feng Chia University prior to his current role. Since 2024, he has been an Assistant Professor with the Department of Communications Engineering, National Chung Cheng University, Chiayi, Taiwan. His research interests include mobile edge computing, UAV networks, and AI for wireless communications. Dr. Lai was a recipient of the Postdoctoral Researcher Academic Research Award from the NSTC, Taiwan, in 2019, and Best Paper Awards at WOCC (2018, 2021) and ICUFN (2015).